Clays and Clay Minerals, Vol. 55, No. 3, 239–252, 2007.

ISOTHERMAL MEASUREMENT OF HEATS OF HYDRATION IN ZEOLITES BY SIMULTANEOUS THERMOGRAVIMETRY AND DIFFERENTIAL SCANNING CALORIMETRY

PHILIP S. NEUHOFF* AND JIE WANG

Department of Geological Sciences, University of Florida, 241 Williamson Hall, Gainesville, FL 32611-2120, USA

Abstract—A calorimetric method for determining isothermal partial and integral heats of hydration reactions ($\Delta\bar{H}_{R,T,P}$ and $\Delta\tilde{H}_{R,T,P}$, respectively) in zeolites and other mineral hydrates is presented. The method involves immersing a dehydrated sample in a humid gas stream under isothermal conditions within a thermal analysis device that records simultaneous differential scanning calorimetric (DSC) and thermogravimetric analysis (TGA) signals. Monitoring changes in sample mass (corresponding to extent of reaction progress) coincident with a quantitative measurement of heat flow allows for direct detection of $\Delta\bar{H}_{R,T,P}$ as a function of the extent of hydration, which can be integrated to determine $\Delta\tilde{H}_{R,T,P}$. In addition, it eliminates uncertainties associated with imprecise knowledge of the starting and final states of a sample during hydration. Measurement under isothermal conditions removes uncertainties associated with heat capacity effects that complicate interpretations of DSC measurements of dehydration heats conducted under traditional scanning temperature conditions. Example experiments on the zeolites natrolite, analcime and chabazite are used to illustrate strategies for quantifying $\Delta\bar{H}_{R,T,P}$ and $\Delta\tilde{H}_{R,T,P}$ and minimizing errors associated with baseline uncertainties. Results from this method agree well with previously published values determined by other calorimetric techniques and regression of phase equilibrium data. In the case of chabazite, the results allowed detailed measurements of the variation in $\Delta\bar{H}_{R,T,P}$ for energetically different water types encountered progressively as the sample absorbed water. This technique complements and in many cases improves the quality of thermodynamic data obtained through phase equilibrium observations and other calorimetric techniques.

Key Words—Analcime, Calorimetry, Chabazite, Enthalpy, Hydration, Natrolite, Thermal Analysis, Thermodynamics, Zeolite.

INTRODUCTION

The capability of many natural and synthetic zeolites to undergo reversible hydration and dehydration is an essential aspect of their technological application and stability in natural and engineered systems. For instance, heat evolution during degassing and rehydration of zeolites is increasingly utilized in heat pump cycles for refrigeration and cooling applications (*e.g.* Boddenberg *et al.*, 2002; Kasai *et al.*, 1994; Petrova *et al.*, 2001; Tchernev, 2001). Partial dehydration of zeolites also plays a critical role in their stability in geological and engineered environments (*e.g.* Bish *et al.*, 2003a; Carey and Bish, 1996; Neuhoff and Bird, 2001; Neuhoff *et al.*, 2000; Wilkin and Barnes, 1998). This is a critical concern in geological radioactive waste repositories in zeolite-rich rock units where equilibria between zeolites and water will play a large role in water heat budgets after waste burial (Bish *et al.*, 2003b; Long and Ewing, 2004; Smyth, 1982). Consequently, there has been considerable interest in developing thermodynamic models of zeolite-water equilibria over the range of temperature and pressure encountered in these environments, particularly with respect to evaluating the heat (enthalpy) evolved during these reactions.

Thermodynamic data necessary to evaluate the hydration states and heats of hydration of zeolites at elevated temperatures and pressures are predominantly derived from: (1) observations of equilibria between zeolites and gaseous water as a function of temperature and water fugacity (*e.g.* Carey and Bish, 1996; Fridriksson *et al.*, 2003; van Reeuwijk, 1974; Wilkin and Barnes, 1999); (2) calorimetric determinations of the heats of formation from heat of solution measurements and transposed temperature drop techniques (*e.g.* Johnson *et al.*, 1982, 1991, 1992; Kiseleva *et al.*, 1996a, 1996b, 1997, 2001; Ogorodova *et al.*, 1996, 2002; Shim *et al.*, 1999; Yang and Navrotsky, 2000; Yang *et al.*, 2001); or (3) direct calorimetric determination of the heat of hydration or dehydration (*e.g.* Boddenberg *et al.*, 2002; Carey and Bish, 1997; Drebushchak, 1999; Fridriksson *et al.*, 2003; Gatta, 1985; Kasai *et al.*, 1994; Mizota *et al.*, 1995; Muller *et al.*, 1998; Petrova *et al.*, 2001). Frequently, inconsistencies are encountered between studies, even on identical or very similar samples (Barrer and Cram, 1971; Bish and Carey, 2001). In part this can be attributed to different reference conditions for defining fully hydrated or dehydrated

* E-mail address of corresponding author:
neuhoff@ufl.edu
DOI: 10.1346/CCMN.2007.0550302

states, especially in systems where excess heats of mixing are present (Bish and Carey, 2001). Resolution of these inconsistencies must rely upon careful accounting for sample water contents before, during and after experiments. While such knowledge is an inherent aspect of phase equilibrium studies, the procedural details of many calorimetric measurements precludes direct knowledge of the state of the sample through the whole measurement process. For example, sample hydration state is typically assessed *ex situ* before, and more rarely after, calorimetric experiments, and complete hydration is often assumed at the end of an experiment. Especially for slow reacting systems, the assumption of complete hydration may be erroneous.

Below we report initial results from a new gas absorption calorimetric technique that employs simultaneous measurement of calorimetric response by differential scanning calorimetry (DSC) and sample mass (taken to represent hydration state) by thermogravimetric analysis (TGA). This technique expands upon previous studies of heats of hydration or dehydration in zeolites and other solid hydrates by DSC and TGA techniques (Drebushchak, 1999; Gatta, 1985; Muller *et al.*, 1998; Pires *et al.*, 2000; van Reeuwijk, 1972) and allows for direct assessment of the hydration state of the sample prior to, after, and during the calorimetric measurement. Example measurements and strategies for interpretation are presented for two zeolites containing only one energetically distinct water site (analcime and natrolite) as well as one that contains multiple, energetically distinct sites (chabazite). The results presented below illustrate the utility of this technique for assessing both partial and integral heats of hydration, with special emphasis on obtaining quantitative heat determinations on samples that contain multiple water types and those that rehydrate slowly.

THEORY

Reversible hydration in zeolites coexisting with a gas phase (*i.e.* where all excess water is present as a vapor) can be represented by chemical equations of the form

$$Z + n\mathrm{H_2O_{(v)}} = Z{\cdot}n\mathrm{H_2O} \quad (1)$$

where $Z{\cdot}n\mathrm{H_2O}$ and Z represent the homologous hydrated and dehydrated forms, respectively, of a zeolite with an aluminosilicate framework and extraframework cation content Z and water content of n water molecules. The corresponding standard states for the zeolite end-members in reaction 1 are unit activity at all temperatures and pressures for the pure phases with water content n (for $Z{\cdot}n\mathrm{H_2O}$) and in the homologous fully dehydrated state (for Z). The standard state for $\mathrm{H_2O_{(v)}}$ is unit fugacity of the pure gas at 1 bar and all temperatures.

The standard change in enthalpy across reaction 1 at temperature T and pressure P, $\Delta H^0_{\mathrm{R},T,P}$, is given by

$$\Delta H^0_{\mathrm{R},T,P} = \Delta H^0_{f(Z{\cdot}n\mathrm{H_2O}),T,P} - \Delta H^0_{f(Z),T,P} - n\Delta H^0_{f(\mathrm{H_2O_{(v)}}),T,P} \quad (2)$$

where $\Delta H^0_{f(i),T,P}$ is the standard enthalpy of formation of species i at T and P. The temperature dependence of $\Delta H^0_{\mathrm{R},T,1\ \mathrm{bar}}$ is given by

$$\Delta H^0_{\mathrm{R},T,1\ \mathrm{bar}} = \Delta H^0_{\mathrm{R},298.15\ \mathrm{K},1\ \mathrm{bar}} + \int_{298.15}^{T} \Delta C^0_{P,\mathrm{R},1\ \mathrm{bar}}\, dT \quad (3)$$

where $\Delta C^0_{P,\mathrm{R},1\ \mathrm{bar}}$ is the standard change in heat capacity, C_P, across reaction 1. The variation in $\Delta H_{\mathrm{R},T,P}$ as a function of progress of reaction 1 can be assessed by noting that this quantity represents the integral heat of reaction ($\Delta\tilde{H}_{\mathrm{R},T,P}$) for complete hydration from an initially anhydrous state; the dependence of $\Delta\tilde{H}_{\mathrm{R},T,P}$ on the extent of hydration is related to the partial molar enthalpy of reaction ($\Delta\bar{H}_{\mathrm{R},T,P}$) by the relation

$$\Delta\tilde{H}_{\mathrm{R},T,P} = \frac{1}{\Theta}\int_0^{\Theta} \Delta\bar{H}_{\mathrm{R},T,P} d\Theta \quad (4)$$

where the integral is performed over the fractional water content, Θ, which is equal to the number of water molecules per formula unit Z at the end of hydration divided by n. Note that $\Delta\bar{H}_{\mathrm{R},T,P}$ is often referred to as the differential heat of reaction by many authors (*e.g.* Gatta, 1985; Pires *et al.*, 2000). For zeolites that contain only one energetically distinct water site, and in the absence of excess heats of mixing between Z and $Z{\cdot}n\mathrm{H_2O}$, the quantities $\Delta\tilde{H}_{\mathrm{R},T,P}$, $\Delta\bar{H}_{\mathrm{R},T,P}$, and $\Delta H^0_{\mathrm{R},T,P}$ are equal when normalized to the same number of water molecules.

Traditional measurements of the enthalpic properties of reaction 1 by DSC have employed dehydration experiments in which the sample is progressively heated at a constant rate (*e.g.* Drebushchak, 1999; van Reeuwijk, 1972). Typical results of such an experiment are shown in Figure 1 for the analcime sample used in this study, along with the simultaneously gathered TGA signal and its first derivative (dTGA). The broad endotherm apparent in the DSC signal in Figure 1

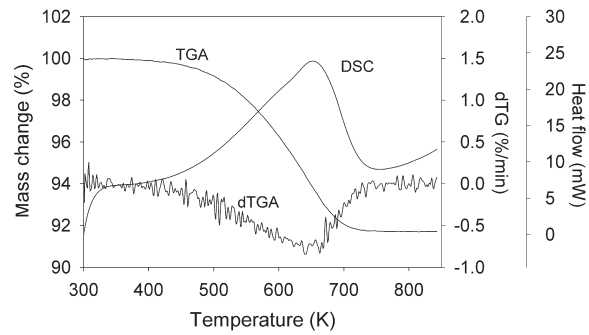

Figure 1. Simultaneously recorded thermogravimetric (TGA) and differential scanning calorimetric (DSC) signals for analcime as a function of temperature. The first derivative of the TG curve is given by the curve labeled dTGA. Data collected at a scanning rate of 15 K/min under ultra-pure N_2.

reflects the heat of dehydration (the inverse of $\Delta H^0_{R,T,P}$ for reaction 1). After caloric calibration, the area of this peak can be used to calculate the heat of dehydration (*e.g.* Drebushchak, 1999; van Reeuwijk, 1974). However, because dehydration proceeds over a protracted range of temperature in such experiments, the DSC signal contains contributions from not only the heat of reaction, but also C_P of the sample. As the stoichiometry of the sample changes progressively during dehydration, the C_P contribution to the DSC curve changes also. This introduces uncertainty in the location of the baseline used to calculate the integral (Muller *et al.*, 1998). In addition, because these reactions are accompanied by a finite $\Delta C_{P,R,1\ bar}$ that is typically on the order of ~4–25 J/K (mole H_2O) (Carey, 1993; Johnson *et al.*, 1982, 1991, 1992), the heats of dehydration vary as a function of temperature. Heats of dehydration measured from scanning dehydration curves such as that shown in Figure 1 are thus averaged over the temperature range of the dehydration event.

An alternative approach is to measure heats of reaction isothermally, which eliminates complications associated with heat capacity effects (Muller *et al.*, 1998). In this approach, the sample is maintained at a constant temperature of interest, and reaction is induced by changing the composition of the gas (*i.e.* changing the water-vapor pressure) within the DSC cell in order to induce hydration or dehydration. Under these conditions, the area of the DSC anomaly during uptake of water vapor is related only to the heat of hydration, as an essentially constant temperature is maintained by the furnace enclosing the sample. One complication is that the extent of reaction (*i.e.* the amount of water taken up by the sample) must be assessed independently. In some cases this has been accomplished by independent (*ex situ)* determinations of the sorption capacity at temperature (*e.g.* Muller *et al.*, 1998). This technique only permits determination of the total integral heat of hydration. An alternative approach is possible in instruments with simultaneous TGA-DSC capabilities. In this case, the water uptake is monitored directly during the experiment by the TGA signal (*e.g.* Pires *et al.*, 2000). This latter approach, which is employed in this study, provides considerably more information about the energetics of the hydration process.

MATERIALS AND METHODS

Materials and sample preparation

Experiments were conducted on phase pure samples of the natural zeolites natrolite, analcime and chabazite. The natrolite sample (NAT001 from Neuhoff *et al.*, 2002) occurs as masses of white crystals filling veins in a metabasaltic tectonic inclusion at the Dallas Gem Mine, San Benito Co., California. The analcime sample (ANA002 from Neuhoff *et al.*, 2003) is from a zeolite-facies metabasalt outcrop at Maniilat on the island of Qeqertarsuaq in West Greenland and prepared from a 1.5 cm euhedral crystal of opaque analcime. The chabazite sample (CHA003 from Neuhoff *et al.*, 2003) occurs in a zeolite-facies metabasalt near Breiddalsheidi, eastern Iceland, as 1 to 2 cm penetration twins of pseudocubic chabazite.

Pure mineral separates were hand picked from slightly crushed megascopic mineral samples and then ground in an agate mortar. Sample purity was confirmed by X-ray powder diffraction (XRPD) and ^{29}Si magic angle spinning nuclear magnetic resonance (MAS NMR) spectroscopy. Sample compositions (Table 1) were determined by electron probe microanalysis (EPMA) at Stanford University on an automated JEOL 733A electron microprobe (see Table 1 for analytical details).

Table 1. Compositions[1] (wt.%) of samples used in study.

	Analcime	Natrolite	Chabazite
SiO_2	56.51	45.54	48.17
Al_2O_3	22.09	26.45	22.27
Fe_2O_3	0.00	0.00	0.00
MnO	0.00	0.00	0.00
MgO	0.01	0.00	0.02
BaO	0.00	0.00	0.00
SrO	0.00	0.11	0.18
CaO	0.01	0.01	11.41
Na_2O	13.54	15.94	0.69
K_2O	0.00	0.00	0.66
Total	92.16	88.05	83.39
H_2O	8.29	9.48	21.82
Formula units			
Si	2.05	2.97	7.75
Al	0.95	2.03	4.22
Fe	0.00	0.00	0.00
Mn	0.00	0.00	0.00
Mg	0.00	0.00	0.00
Ba	0.00	0.00	0.00
Sr	0.00	0.00	0.02
Ca	0.00	0.00	1.97
Na	0.95	2.02	0.22
K	0.00	0.00	0.14
O	6.00	10.00	24.00
H_2O	1.01	2.01	12.39
Si/Al	2.17[2]	1.46	1.84
Σ (2Ca+Na+K)	0.95	2.02	4.31

[1] Sample compositions were determined by electron probe microanalysis (EPMA) at Stanford University on an automated JEOL 733A electron microprobe operated at 15 kV accelerating potential and 15 nA beam current. Calibration was conducted using natural geological standards. Beam widths were 30 μm depending on grain size. Raw counts were collected for 20 s and converted to oxide weight percents using the CITZAF correction procedure after accounting for unanalyzed oxygen (Tingle *et al.*, 1996). H_2O contents determined by TGA.

[2] Analysis of the framework content of this sample by ^{29}Si magic-angle spinning nuclear magnetic resonance spectroscopy (Neuhoff *et al.*, 2003) indicates that the Si/Al ratio in this sample is 2.09; the composition listed in Table 3 is based on this value.

Thermal analysis and calorimetry

Calorimetric experiments were conducted on a Netzsch STA 449C Jupiter simultaneous DSC-TGA apparatus. Gas flow was maintained at ~30 mL/min using mass flow controllers. All experiments were conducted in Pt-Rh crucibles with unsealed, perforated lids. Two types of experiments were conducted. The first consisted of standard dynamic heating thermal analysis from ambient temperature to 1023 K at 15 K/min. The second consisted of isothermal heat of absorption measurements. The typical temperature program for the latter measurements consisted of four steps: (1) an initial 15 K/min heating step in which the sample was completely dehydrated in the presence of dry, ultra-pure N_2; (2) cooling under dry gas to the experimental temperature; (3) equilibration (10−30 min) under dry gas at the experimental temperature until both the DSC and TGA baselines stabilized; and (4) introduction of humidity into the gas stream and reaction until the DSC and TGA baselines stabilized, signaling the end of reaction. Humidity was added to the gas stream during hydration by bubbling ultra-pure N_2 gas through a saturated NaCl solution at room temperature. Mixing of a dry protective gas (introduced near the base of the microbalance) and the humidified gas into the sample chamber resulted in an average humidity of 11−14 mbar during hydration steps (humidity was monitored continuously on the gas stream exiting the system using a flow-through humidity meter manufactured by Sable Systems).

Temperature and caloric calibrations were conducted using data based on the DSC response of standard materials. A multipoint temperature calibration curve was developed using the melting points of H_2O, Ga, In, Sn, Bi, Zn and Al along with the solid-solid transition points of CsCl and quartz (Cammenga *et al.*, 1993; Gmelin and Sarge, 2000; Hohne *et al.*, 1990; Sabbah *et al.*, 1999). Due to the incompatibility of these materials with the Pt-Rh crucible used in the experiments, temperature calibration was conducted in identical crucibles lined with a sub-mm thick insert of alumina.

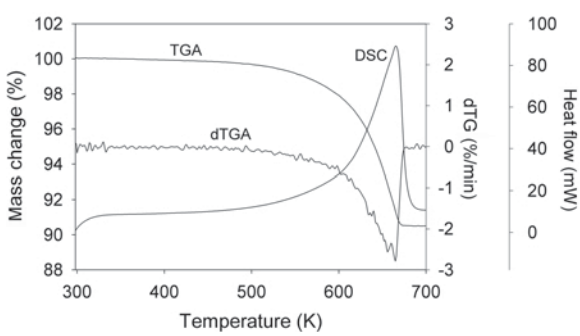

Figure 2. Simultaneously recorded TGA and DSC signals for natrolite as a function of temperature. Data collected at a scanning rate of 15 K/min under ultrapure N_2. See caption for Figure 1 for abbreviations.

Caloric calibration was accomplished by the heat-flow rate method (Gmelin and Sarge, 2000) using the DSC response of synthetic sapphire (Gmelin and Sarge, 2000; Sabbah *et al.*, 1999; Sarge *et al.*, 1994; Stolen *et al.*, 1996). The background-corrected DSC response of a synthetic sapphire disc similar in mass to the experimental charges was measured at heating rates of 5, 10, 15 and 20 K/min over the range of temperatures encountered in this study. Caloric calibration factors calculated from results at each heating rate agreed within 1% and were a nearly linear function of temperature.

RESULTS AND DISCUSSION

Natrolite

Each channel in natrolite contains two Na^+ ions and two water molecules with each cation site and each water site being symmetrically equivalent (*e.g.* Alberti and Vezzalini, 1981; Alberti and Vezzalini, 1983; Meier, 1960; Pechar *et al.*, 1983). It thus appears likely that all water molecules in natrolite are energetically similar. This is consistent with observations from thermal analysis such as those shown in Figure 2; water loss from the sample is accompanied by only a single peak in both the DSC and dTGA signals. After an initial phase of gradual water loss, dehydration proceeds abruptly over a narrow range of temperature.

Figure 3 shows the results of an isothermal water vapor absorption experiment on dehydrated natrolite at 432 K. The natrolite sample was only heated to 673 K in order to avoid formation of the β phase of dehydrated natrolite that forms irreversibly at higher temperature (Baur and Joswig, 1996; van Reeuwijk, 1972, 1974). After equilibration of a dehydrated sample at temperature under dry N_2 flow (signaled by a constant baseline for both the DSC and TGA signals shown in the gray region), the atmosphere was switched to a stream of humidified N_2. The total time lag between dehydration

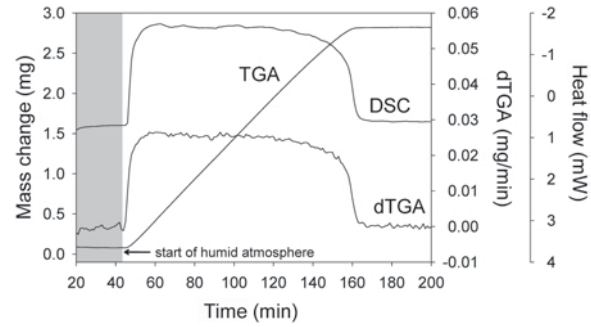

Figure 3. Gas absorption calorimetric experiment on natrolite conducted at 432 K and 1300 mbar vapor pressure. The area of the figure encompassed by the gray box denotes initial equilibration of sample at experimental temperature under dry N_2. The rest of the experiment was conducted in the presence of a flow of humidified N_2. See Figure 1 for explanation of the symbols.

and the start of rehydration was ~130 min. The sample immediately started to absorb water, which is manifested by abrupt changes in both the DSC and TGA signals. The TGA signal increases monotonically during hydration until leveling off after the reaction was complete. Total water uptake during the experiment was ~9.1%, somewhat less than the ~10.5% expected for complete hydration. It is unclear to what extent this reflects the equilibrium water content of natrolite at this temperature and water-vapor pressure (both the water-vapor pressure, ~1200 mbar, and the total gas pressure, 1 bar, are well below the saturated vapor pressure at this temperature, ~6 bar) or a decrease in sorption capacity due to dehydration as noted in some zeolites (*e.g.* Fialips *et al.*, 2005). The rate of absorption is reflected in the dTGA signal; in this case, the rate of mass change increases abruptly at the beginning of the experiment and then stays relatively constant until the reaction ceases. The relatively constant rate of hydration during the course of the experiment is suggestive of zero-order kinetics, as observed previously during hydration of this mineral (Otsuka *et al.*, 1991). The behavior of the DSC signal mirrors that of the dTGA curve almost exactly, in this case decreasing abruptly due to the exothermic nature of the reaction (in fact, the temperature of the sample rises by 0.2−0.3 K during hydration), then staying relatively constant with some undulation until cessation of the reaction. Repeated cycling of the same sample through the dehydration and rehydration steps of this procedure led to a progressive decrease in sorption capacity.

The results shown in Figure 3 can be used to directly assess $\Delta\tilde{H}_{R,T,P}$ (normalized to one mole of H_2O absorption) from the area of the DSC peak (A; in μVs) through the relation

$$\Delta\tilde{H}^0_{R,T,P} = kA(\Delta m)^{-1}\,(MW_{H_2O}) \quad (5)$$

where k is the caloric calibration factor (in W/μV; note that this is already factored into the results shown in Figure 3), Δm is the mass change measured by TGA, and MW_{H_2O} is the molecular weight of water. The results of this calculation are shown in Table 2 (−98.0±1.0 kJ/mol) along with various determinations of $\Delta\tilde{H}_{R,T,P}$ from the literature. It can be seen in Table 2 that data from this technique agree within error with those of Guliev *et al.* (1989) determined by immersion calorimetry at a similar temperature. Although the other values for $\Delta\tilde{H}_{R,T,P}$ listed in Table 2 were obtained at temperatures either significantly lower or higher than those in this study (and thus might be expected to deviate from our results and those of Guliev *et al.* (1989) if the heat capacity change across the reaction is non-negligible), all are similar in magnitude (and mostly within error) to the results from this study.

The striking similarity in curve shape between the DSC and dTGA signals in Figure 3 suggests that these signals are strongly correlated (in fact, linear regression of these two signals against each other produced an R^2 value of 0.995). This suggests that $\Delta\tilde{H}_{R,T,P}$ and $\Delta\bar{H}_{R,T,P}$ are insensitive to Θ and should be similar in magnitude. Due to the fact that both the extent of reaction and the heat evolved during reaction are simultaneously recorded in this experiment, the data in Figure 3 can be used to directly assess $\Delta\tilde{H}_{R,T,P}$. Figure 4 shows the total heat evolved during the course of the experiment as a function of mass absorbed; these data are linearly related (R^2 indistinguishable from 1.0). The slope of the linear regression shown in Figure 4 represents the average $\Delta\bar{H}_{R,T,P}$ over the course of the experiment, and is in excellent agreement with $\Delta\tilde{H}_{R,T,P}$ (Table 2). Figure 5 shows $\Delta\bar{H}_{R,T,P}$ during the course of this

Table 2. Enthalpy of hydration of natrolite.

Composition	Method[1]	Temperature (K)	$\Delta\tilde{H}_{R,T,P}$ (kJ/mol H_2O)
$(NaAl)_2Si_2O_{10}\cdot 2H_2O$	TTD	298.15	−101.7±3.6[2]
$(NaAl)_2Si_2O_{10}\cdot 2H_2O$	PE	900	−108[3]
not reported	PE	684.15	−102.9±4.0[4]
not reported	DSC	623.15	−89.1[5]
$(NaAl)_2Si_2O_{10}\cdot 2H_2O$	IM	453.15	−100.0±5.0[6]
$(NaAl)_2Si_2O_{10}\cdot 2H_2O$	DSC-I	432	−98.0±1.0[7]
$(NaAl)_2Si_2O_{10}\cdot 2H_2O$	DSC-PE	432	−97.6±1.0[7]

[1] Methods − HF: determination of enthalpies of formation of hydrated and dehydrated homologs by HF solution calorimetry; TTD: transposed temperature drop calorimetry; PE: retrieval from phase equilibrium observations; DSC: calculated from scanning DSC measurement; IM: heat of immersion in water; DSC-I: integral heat of hydration from water-vapor measurement by DSC calculated from peak area; DSC-PE: average partial enthalpy of hydration from water vapor calculated from finite difference derivatives of DSC and DTGA signals.
[2] Kiseleva *et al.* (1997)
[3] Hey (1932)
[4] van Reeuwijk (1974)
[5] van Reeuwijk (1972)
[6] Guliev *et al.* (1989)
[7] This study

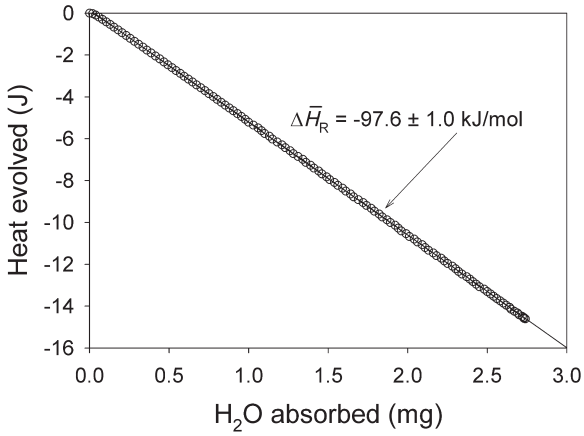

Figure 4. Cumulative heat evolved during absorption of water into natrolite as a function of mass absorbed calculated from the experimental data shown in Figure 3. The error on each data-point is smaller than the symbol.

experiment calculated by taking finite difference derivatives of the area under the DSC curve in Figure 3 with respect to the mass change given by the concurrent TGA signal. With the exception of the very beginning of the hydration reaction (*i.e.* at low values of $X_{\text{hydrated natrolite}}$), $\Delta\tilde{H}_{R,T,P}$ undulates around the value found by linear regression of the data in Figure 4.

The relatively less energetic values at the very beginning of the hydration step probably do not reflect the energetics of hydration in natrolite, but rather are related to some other phenomenon occurring at the beginning of the reaction. In general, water molecules incorporated into zeolites at low degrees of hydration are more energetic (stable) than those entering the structure at higher water contents (*e.g.* Carey and Bish, 1996; Fialips *et al*., 2005) rather than the distinctly non-energetic water values depicted in Figure 5. This phenomenon, which is clearly anomalous, precludes quantification of $\Delta\tilde{H}_{R,T,P}$ at very low degrees of infilling. The net effect on $\Delta\tilde{H}_{R,T,P}$ is minimal in this case, however, as this portion of the DSC response only accounts for a few tenths of a percent of the total heat evolved.

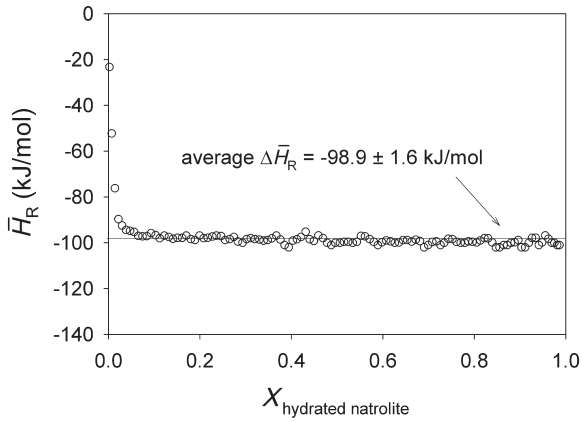

Figure 5. Partial molar enthalpy of hydration ($\Delta\tilde{H}_{R,T,P}$) as a function of the mole fraction of hydrated natrolite ($X_{\text{hydrated natrolite}}$) calculated by taking finite difference derivatives of the experimental results shown in Figure 3. The average $\Delta\tilde{H}_{R,T,P}$ shown by the horizontal line in the figure is the mean of the data for $X_{\text{hydrated natrolite}}$ >0.1. The error on each data point is smaller than the symbol.

There are several possible explanations for the non-energetic results obtained at low degrees of infilling. The first is that the initial uptake of water involves some distinctly non-energetic species like adsorbed water. While there may be some component of heat of adsorption onto the natrolite surface at the induction of the hydration step recorded in this signal, it is important to note that the DSC signal changes before the TGA signal does during the reaction. As surface adsorption would still involve an increase in mass, this suggests that some process is occurring in the sample prior to a detectable mass gain. A second possibility is that the earlier induction of the DSC signal might reflect a lag in the TGA signal relative to the DSC signal. However, in the current experimental setup, the reverse is more likely as the mass change is recorded instantaneously, while one might expect heat transport through the sample to produce a lag in the heat signal. The early induction of the DSC signal also contradicts the possibility that thermal lag in the DSC signal (which would produce an apparent low heat signal per change in mass) is not the cause of the non-energetic values. Our preferred explanation is that the initial absorption of H_2O is coupled to another, less energetic, process. A likely candidate is exchange of N_2 for H_2O at low degrees of hydration, which would potentially result in only a minimal net mass change until the rate of hydration significantly outpaces the loss of N_2 (or the latter is completely purged from the zeolite channels). Positive enthalpy of desorption of N_2 from natrolite (−37 kJ/mol N_2; Neuhoff and Wang, 2007) would offset the negative enthalpy of hydration, causing the overall heat effect to be less negative, as observed (Figure 5).

Analcime

Analcime at full hydration contains water molecules distributed across only one crystallographic site both at room temperature (*e.g.* Mazzi and Galli, 1978) and at elevated temperatures during dehydration (Cruciani and Gualtieri, 1999). During heating of analcime (Figure 1) these water molecules are lost during a single, but protracted dehydration event accompanied by a single peak in both the DSC and dTGA signals. This is consistent with lead borate solution calorimetric observations that there is little or no excess enthalpy of mixing between hydrated and dehydrated analcime (Ogorodova *et al.*, 1996) suggesting that all water molecules in analcime are energetically similar. Consequently, it appears that $\Delta\tilde{H}_{R,T,P}$ and $\Delta\tilde{H}_{R,T,P}$ in analcime should be equivalent over the whole range of

solution between the dehydrated and hydrated end-members.

Results of an isothermal (490 K) hydration experiment are shown in Figure 6 for the same sample of analcime as depicted in Figure 1. The sample was dehydrated by scanning heating to 745 K, and total time lag between dehydration and the hydration step in Figure 6 was ~130 min. After introduction of H_2O vapor, the sample immediately started to absorb water, leading to abrupt changes in both the DSC and TGA signals. The initially relatively rapid (dTGA is relatively large) rate of hydration begins to decrease shortly after reaction starts. After ~160 min of reaction with the humid atmosphere, the reaction had slowed to a point where the DSC signal decayed to near baseline levels and was essentially invariant with respect to time even though the sample continued to absorb H_2O (the TGA signal continued to increase) through the cessation of the experiment 850 min later. The slow rate of the reaction at this point is reflected in the near-zero value of dTGA. During the portion of the experiment shown in Figure 6, the sample reabsorbed ~4.5% of its mass (and only 5.6% at the cessation of the experiment), as opposed to ~9.1% mass gain expected for complete rehydration. Repeated tests on the same sample indicate that our analcime sample can be reversibly dehydrated and rehydrated without loss of sorption capacity or changes in hydration energetics.

The slow rehydration rate exhibited by analcime, which has been noted previously (Chipera and Bish, 1991), presents considerable complications for quantifying the enthalpy of reaction. Because the reaction effectively never goes to completion, a stable DSC baseline is not established at the end of the experiment for use as a basis for integrating the area under the curve. The change in gas input at the beginning of the hydration step leads invariably to some fluctuations in signals and, in some cases, a change in both the TGA and DSC baselines that is quantitatively important. One way around this problem in materials such as analcime, for which there is no excess enthalpy of mixing across the hydrated-dehydrated analcime solid-solution, is to take advantage of the fact that the DSC signal and the dTGA signals are strongly correlated, as can be seen in Figure 6. These signals are plotted against each other in Figure 7. The strong correlation (R^2 = 0.998) indicates that, as is also the case in natrolite, the dependence of the background-corrected DSC signal on dTGA is directly proportional to $\Delta\bar{H}_{R,T,P}$. This value is represented by the slope of the regression line through the data of Figure 7. In addition, the y intercept of this regression represents the DSC signal when dTGA = 0; *i.e.* the baseline at the end of reaction. The value of $\Delta\bar{H}_{R,T,P}$, consistent with the regression in Figure 7, is given in Table 3 along with values of $\Delta\tilde{H}_{R,T,P}$ for analcime from the literature. It can be seen that the data in Figures 6 and 7, if one assumes that $\Delta\bar{H}_{R,T,P}$ and $\Delta\tilde{H}_{R,T,P}$ are equivalent, are in excellent agreement with previous studies.

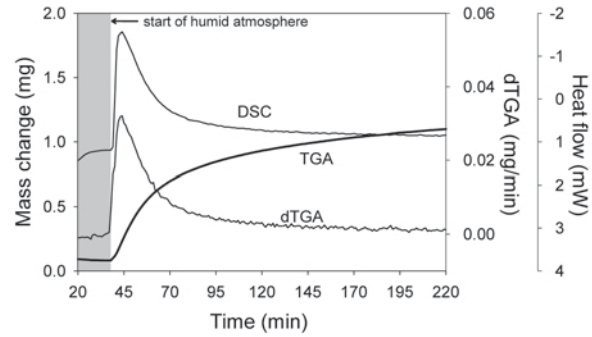

Figure 6. Gas absorption calorimetric experiment on analcime conducted at 490 K and 1400 mbar vapor pressure. The area of the figure encompassed by the gray box denotes initial equilibration of the sample at experimental temperature under dry N_2. The rest of the experiment was conducted in the presence of a flow of humidified N_2. See the caption of Figure 1 caption for an explanation of the symbols.

The data of Figures 6 and 7 were used to calculate cumulative heat evolved as a function of mass absorbed (Figure 8) and $\Delta\bar{H}_{R,T,P}$ as a function of the mole fraction of hydrated analcime ($X_{\text{hydrated analcime}}$; Figure 9) in a manner similar to the natrolite example shown above. These calculations required assumption of a baseline for the DSC curve, which was taken to be the y intercept of the regression line in Figure 7. From Figure 8 it can be seen that there is excellent linear correlation between the cumulative area under the DSC curve and the amount of H_2O absorbed (R^2 indistinguishable from 1.0), suggesting that no excess heat of mixing over the range of water contents produced in this experiment. As in the case of natrolite, $\Delta\bar{H}_{R,T,P}$ at low degrees of absorption is less energetic than observed at higher degrees of absorption. This portion of the experiment accounts for ~1% of the total heat evolved during the reaction. While this effect

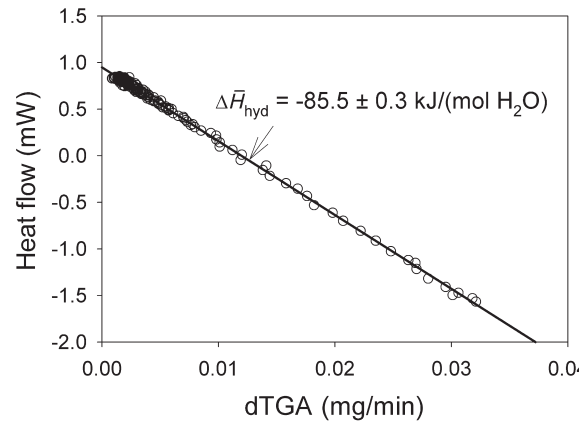

Figure 7. Plot of the heat flow (DSC signal) *vs.* dTGA for the experimental results shown in Figure 5. The slope of the linear regression shown in the figure corresponds to $\Delta\bar{H}_{R,T,P}$.

Table 3. Enthalpy of hydration of analcime.

Composition	Method[1]	Temperature (K)	$\Delta\tilde{H}_{R,T,P}$ (kJ/mol H_2O)
$(NaAl)_{0.96}Si_{2.04}O_6{\cdot}H_2O$	HF	298.15	−84.9±4.0[2]
$(NaAl)_{0.95}Si_{2.05}O_6{\cdot}H_2O$	TTD	298.15	−85.7±1.9[3]
$(NaAl)_{0.96}Si_{2.04}O_6{\cdot}H_2O$	HF	298.15	−73.9±4.4[4]
$NaAlSi_2O_6{\cdot}H_2O$	PE	298.15	−80.4[5]
not reported	PE	569.15	−83.7 ± 4.0[6]
	PE	660.15	−86.6±4.0[6]
$(NaAl)_{0.97}Si_{2.03}O_6{\cdot}1.015H_2O$	DSC-PE	490.15	−85.5±0.3[7]
$(NaAl)_{0.97}Si_{2.03}O_6{\cdot}1.015H_2O$	DSC-APE	490.15	−85.5±2.1[7]

[1] Methods: see footnote to Table 2 plus DSC-APE: partial molar enthalpy of hydration from water vapor calculated from correlation between DSC and dTGA
[2] Johnson *et al.* (1982)
[3] Ogorodova *et al.* (1996)
[4] Calculated from data of Barany (1962) as recalculated by Johnson *et al.* (1982)
[5] Retrieved by Bish and Carey (2001) from observations of Balgord and Roy (1973)
[6] van Reeuwijk (1974)
[7] This study; $\Delta\bar{H}_{R,T,P}$ taken as equal to $\Delta\bar{H}_{R,T,P}$ (see text)

is large enough to significantly affect the quality of $\Delta\tilde{H}_{R,T,P}$ data calculated from this experiment, it does not influence calculation of $\Delta\bar{H}_{R,T,P}$. In fact, the average value of $\Delta\bar{H}_{R,T,P}$ consistent with the bulk of the data in Figure 9 is in excellent agreement with that obtained from the regression in Figure 8 (Table 3).

Chabazite

Unlike analcime and natrolite, water molecules within the structure of chabazite are distributed over several (up to seven depending on the cation contents and the refinement; *e.g.* Alberti *et al.*, 1982; Gualtieri, 2000) crystallographically distinct sites. These sites differ in both their position within the channel structure of chabazite and in the number of extraframework cations in their coordination shell. Consequently, different water molecules in the chabazite structure are likely to be energetically distinct. This is borne out by results of both thermal analysis and thermodynamic analysis of chabazite dehydration (*cf.* Valueva and Goryainov, 1992; Fialips *et al.*, 2005). Figure 10 shows the results of a scanning-heating dehydration of the chabazite sample used in this study. Although the mass appears to decrease continuously with increasing temperature, inspection of the DSC signal suggests the presence of three separate dehydration events during this experiment: a prominent peak centered around 450 K corresponding to the steepest part of the TGA curve, a considerably less prominent peak in the vicinity of 780 K and a small shoulder on the low-temperature side

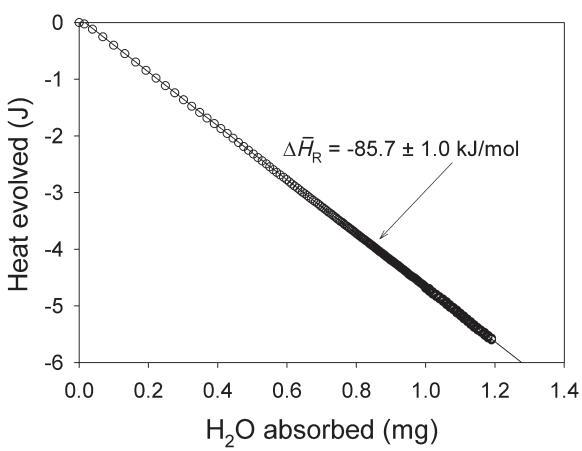

Figure 8. Cumulative heat evolved during absorption of water into analcime as a function of mass absorbed calculated from the experimental data shown in Figure 6. The error on each data point is smaller than the symbol.

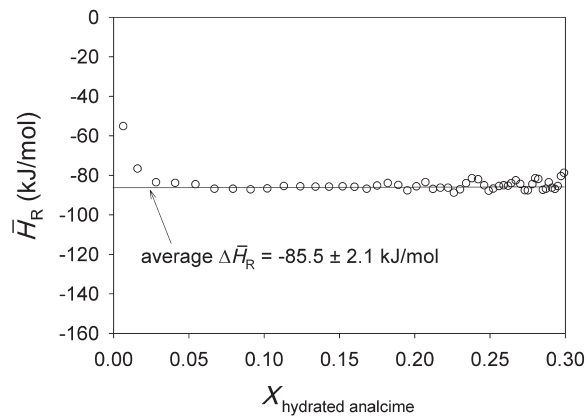

Figure 9. Partial molar enthalpy of hydration ($\Delta\bar{H}_{R,T,P}$) as a function of the mole fraction of hydrated analcime ($X_{\text{hydrated analcime}}$) calculated by taking finite difference derivatives of the experimental results shown in Figure 5. The average $\Delta\bar{H}_{R,T,P}$ shown by the horizontal line in the figure is the mean of the data for $X_{\text{hydrated natrolite}}$ >0.05. The error on each data-point is smaller than the symbol.

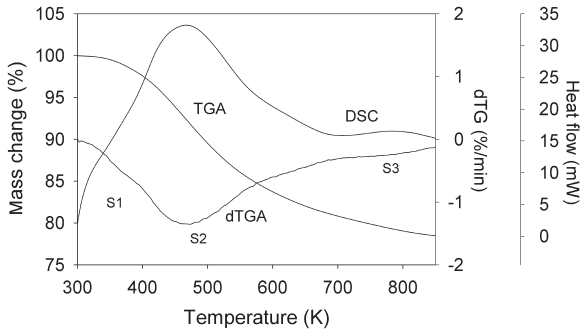

Figure 10. Simultaneously recorded TGA and DSC signals for chabazite as a function of temperature. The data were collected at a scanning rate of 15 K/min under ultra-pure N_2. See the caption of Figure 1 for abbreviations. Symbols S1, S2 and S3 refer to water types discussed by (Fialips *et al.*, 2005).

of the main peak in the vicinity of 400 K. These features are also expressed to varying degrees in the dTGA signal shown in Figure 10. These three dehydration features are also observed in the stepwise behavior of the heat of hydration and Raman spectra as a function of water content (Valueva and Goryainov, 1992) and variations in sorption isotherms as a function of water content (Fialips *et al.*, 2005). The latter authors used this inference to develop a three-site thermodynamic model to describe the dehydration behavior of chabazite (the sites being named S1, S2 and S3 with S1 corresponding to water molecules associated with the feature at 400 K in Figure 10, S2 the feature at 450 K, and S3 the dehydration step centered at 780 K). The relationship of these water types to the distinct crystallographic sites observed in refinements of the chabazite structure is unclear.

The results of an isothermal hydration experiment at 374 K on the chabazite sample from this study are shown in Figure 11. The sample was dehydrated by scanning heating to 980 K, followed by a time lag of ~170 min prior to rehydration. Total water uptake during

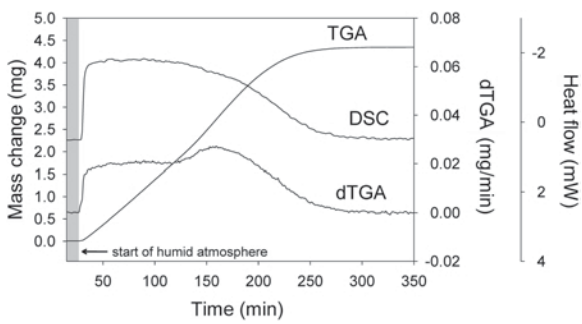

Figure 11. Gas absorption calorimetric experiment on chabazite conducted at 374 K, and 1100 mbar vapor pressure. The area of the figure encompassed by the gray box denotes initial equilibration of the sample at experimental temperature under dry N_2. The rest of the experiment was conducted in the presence of a flow of humidified N_2. See Figure 1 for an explanation of the symbols.

this experiment was only ~16.2% of the initial hydrated mass of the chabazite, in contrast to ~21.8% total mass loss during the experiment shown in Figure 10. This is consistent with the equilibrium observations of Fialips *et al.* (2005) who observed ~75% hydration under similar temperature-humidity conditions. Based on comparison with Figure 10, and the calculations of Fialips *et al.* (2005), the water content attained in the experiment shown in Figure 11 should reflect occupancy of S2 and S3 but probably not S1. Repeated tests on the same sample indicate that our chabazite sample can be reversibly dehydrated and rehydrated without loss of sorption capacity or changes in hydration energetics. Unlike the natrolite and analcime experiments shown in Figures 3 and 6, there is a marked departure in curve shape between the DSC and dTGA signals that suggests that $\Delta\bar{H}_{R,T,P}$ is a function of water content during the sample. While the DSC signal decreases steadily after the initial induction of the experiment (slowly at first, and then more rapidly after ~150 min), the rate of mass change increases abruptly at ~125 min, leading to a secondary peak in the dTGA curve. The net consequence of these two contrasting behaviors is that $\Delta\bar{H}_{R,T,P}$ must become less energetic with progress of the reaction in light of the decreasing DSC signal and increasing dTGA signal.

Calculated values of $\Delta\bar{H}_{R,T,P}$ determined by taking finite difference derivatives of the dTGA curve and the area under the DSC curve in Figure 11 are shown in Figure 12. Determinations of $\Delta\bar{H}_{R,T,P}$ as a function of water content from Fialips *et al.* (2005), Shim *et al.*

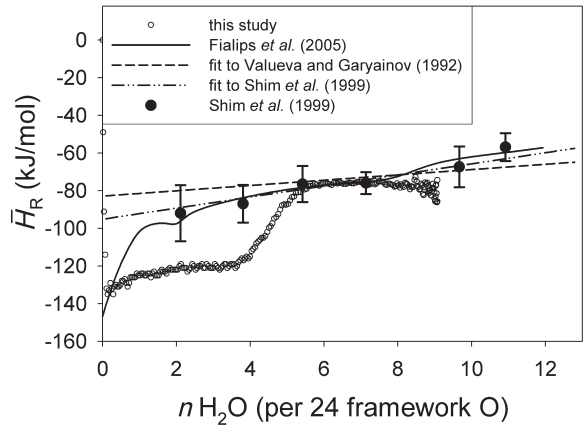

Figure 12. Partial molar enthalpy of hydration ($\Delta\bar{H}_{R,T,P}$) of chabazite as a function of the number of water molecules per 24 framework oxygens. Open symbols calculated by taking finite difference derivatives of the experimental results shown in Figure 10. Closed symbols with error bars are 'model independent' partial molar enthalpies of hydration calculated from transposed temperature drop calorimetric observations on a Ca-rich chabazite by Shim *et al.* (1999). Calculation procedures used to derive the curves describing the data of Shim (1999), Valueva and Goryainov (1992) and Fialips *et al.* (2005) are discussed in the text. The error on each data point is smaller than the symbol.

(1999), and Valueva and Goryainov (1992) are shown for comparison. The curves representing the results of Shim *et al.* (1999) and Valueva and Goryainov (1992) are calculated from regressions reported by Shim *et al.* (1999). These curves and the data points of Shim *et al.* (1999) were adjusted from a liquid water reference state at 298.15 K to a water-vapor reference state at 374 K by accounting for the enthalpy of vaporization of water reported by Robie and Hemingway (1995) and the heat capacity of reaction, taken to be 3R (where R is the gas constant) independent of temperature as proposed by Fialips *et al.* (2005). The heat capacity correction makes the data of Shim *et al.* (1999) and Valueva and Goryainov (1992) ~1.8 kJ/mol H_2O less stable (*i.e.* have a greater value of $\Delta\bar{H}_{R,T,P}$). The curve representing the data of Fialips *et al.* (2005) was calculated at 374 K using the regressed thermodynamic properties and equations presented by these authors (calculation kindly supplied by J.W. Carey).

The data shown in Figure 12 from this study clearly indicate the presence of energetically-distinct water types in chabazite. After the initial induction phase of the experiment, in which $\Delta\bar{H}_{R,T,P}$ decreases rapidly from very non-energetic values (presumably representing the same phenomena as observed above in natrolite and analcime), the data appear to indicate sequential absorption of water into two energetically distinct sites. The first occurs between water contents of 0 and 4 water molecules per mol of chabazite, for which $\Delta\bar{H}_{R,T,P}$ increases gradually from ~−133 kJ/mol of H_2O to ~−117 kJ/mol. Between water contents of ~4 and ~5.5 water molecules per mol, $\Delta\bar{H}_{R,T,P}$ increases more rapidly to ~−77 kJ/mol, where it stays relatively constant until reaction ceases. The scatter in the data at the highest water contents is a consequence of the relatively large errors associated with integrating and differentiating the small DSC and dTGA signals, respectively, at the end of the experiment. The transition from the more stable water type encountered at low degrees of loading to the less stable water at higher degrees of loading is not apparent in the DSC signal in Figure 11, but corresponds to the sudden increase in dTGA at ~125 min in the experiment. By comparison with the results shown in Figure 10 and the observations of Fialips *et al.* (2005), it appears that the more stable water type probably roughly corresponds to S3, and the less stable water type is S2. However, as discussed below, the relative proportions of S3 and S2 in our sample is significantly different than in that of Fialips *et al.* (2005). As suggested by the calculations of Fialips *et al.* (2005), the third, and least stable, water type (S1) did not absorb in appreciable amounts under the conditions employed in this experiment.

In general, the results from this study shown in Figure 12 agree well with those from previous calorimetric studies at relatively high degrees of hydration but differ significantly at low degrees of hydration. At between 6 and 8 water molecules per mol, our data are essentially coincident with those of previous studies. Even though these four different datasets were generated through four different techniques (*i.e.* DSC-based gas absorption calorimetry in this study, transposed temperature drop (TTD) calorimetry by Shim *et al.* (1999), traditional immersion calorimetry by Valueva and Goryainov (1992), and phase equilibrium observations by Fialips *et al.* (2005)), they all give remarkably similar results for water contents over which data from each study were constrained. However, the four datasets disagree markedly at lower water contents, with the results of this study and that of Fialips *et al.* (2005) being considerably more exothermic than those of Valueva and Goryainov (1992) and Shim *et al.* (1999). As discussed by Fialips *et al.* (2005), the discrepancy between the regressed results of Shim *et al.* (1999) and those of their study and ours is probably due to a lack of constraints at very low water contents in the transposed temperature drop results. The discrepancy between the data of Valueva and Goryainov (1992) and this study are less easy to explain.

Valueva and Goryainov (1992) determined $\Delta\tilde{H}_{R,T,P}$ directly at low water contents (from 0 to 7 mol H_2O per mol chabazite) through measurements of the heat of immersion in liquid water. Their data are very similar to the immersion calorimetric results of Barrer and Cram (1971) down to water contents of ~2 mol H_2O per formula unit (see comparison in Fialips *et al.*, 2005). Barrer and Cram's (1971) results indicate that $\Delta\tilde{H}_{R,T,P}$ is relatively invariant when the sample is hydrated from initial water contents of ~0−2 mol H_2O per mol chabazite to complete hydration. Fialips *et al.* (2005) suggested that the disparity between the results of earlier calorimetric studies and the regressed parameters from their study was a consequence of irreversible changes to chabazite during the preparation of the dehydrated sample. The dehydrated sample in this study was prepared under similar conditions to those of Valueva and Goryainov (1992) and Barrer and Cram (1971), yet exhibits considerably more exothermic results than those obtained in the earlier calorimetric studies and exhibits no loss in sorption capacity after dehydration. Thus, our sample is not irreversibly modified to the extent that earlier samples were, or the explanation lies elsewhere.

It is important to note that the discrepancy noted by Fialips *et al.* (2005) between their sample and those of previous studies was most pronounced in calculated values of $\Delta\bar{H}_{R,T,P}$ and was less pronounced in $\Delta\tilde{H}_{R,T,P}$. The significant discrepancy between $\Delta\bar{H}_{R,T,P}$ determined from previous calorimetric results and those of Fialips *et al.* (2005) and this study in large part reflects the model-dependent nature of this property as regressed from raw $\Delta\tilde{H}_{R,T,P}$ such as those obtained by immersion or TTD calorimetry. The form of equation used to regress the compositional dependence of $\Delta\bar{H}_{R,T,P}$ may well lead to erroneously less negative values, especially where constraints at low degrees of filling are sparse. When the raw

$\Delta\bar{H}_{R,T,P}$ calorimetric results are compared to the calculated values of Fialips *et al.* (2005), the discrepancy is considerably smaller and largely restricted to samples that were rehydrated from a completely dehydrated state (*cf.* Figure 11 in Fialips *et al.*, 2005; a similar analysis is not possible with the data of the current study as full hydration was not achieved). It is important to note that the discrepancy between the immersion calorimetric results and those of Fialips *et al.* (2005) decreases considerably as the degree of infilling increases, and that the immersion calorimetric results of Barrer and Cram (1971) indicate a negligible heat of hydration below water contents of 2 mol of H_2O per formula unit. One possible explanation for these observations may lie in the phenomenon causing the relatively non-energetic values of $\Delta\bar{H}_{R,T,P}$ at the start of the hydration reaction (Figure 11). If this phenomenon is related to exchange of H_2O for N_2 as suggested above, the heat effect should be present in any calorimetric heat of hydration measurement. This effect would preferentially affect $\Delta\tilde{H}_{R,T,P}$ measured at low degrees of infilling, causing these values to appear less negative as the relatively low enthalpy effects at the beginning of reaction would be averaged with the very energetic water molecules that initially absorb into chabazite. This may in part explain the discrepancy between the results of this study (and Fialips *et al.*, 2005) and the immersion calorimetric results of Barrer and Cram (1971) and Valueva and Goryainov (1992). Other possibilities exist, however, including irreversible modification during dehydration and inter-sample differences that can only be resolved through study of the same sample by different techniques.

Comparison between the results of this study and those of Fialips *et al.* (2005) is complicated by differences in sample composition and the assumptions used to plot the latter data. The sample used in this study is considerably more Si- and Ca-rich than that used by Fialips *et al.* (2005), which will undoubtedly affect the energetics of water in the samples, the relative abundances of different water types, and potential irreversible transformation of the chabazite structure upon dehydration (Bish and Carey, 2001). In addition, the representation of the results of Fialips *et al.* (2005) in Figure 12 assumes an equilibrium distribution of water molecules for each water content (calculated by varying the vapor pressure at temperature). Sorption of H_2O from the gas phase into chabazite in the present study is a non-equilibrium process, and equilibrium is only possible at the end of the reaction. Compositional variations and equilibrium *vs.* non-equilibrium distributions of energetically distinct water molecules undoubtedly affect the relative magnitudes of $\Delta\bar{H}_{R,T,P}$ as a function of water content between these two studies. Nonetheless, both studies indicate a component of step-wise change in $\Delta\bar{H}_{R,T,P}$ as the nature of the water sites changes with increasing hydration, in contrast to the interpreted behavior of the immersion and TTD calorimetric data in Figure 12. However, our results in Figure 12 indicate significant differences between both the abundance and energetics of S3 water in chabazite. The regression presented by Fialips *et al.* (2005) suggests a maximum content of S3 water in chabazite of ~1.8 molecules per mol, in contrast with the results of our study which suggest that this site is at least twice as abundant. As noted above, the crystallographic nature of the water-type-I chabazite is not resolved. However, Valueva and Goryainov (1992) observed a difference in the nature of water below and above 3.8 water molecules per formula unit in Raman spectra of variously hydrated chabazites. This change in behavior probably represents a change from chabazites containing only S3 water (below 3.8 water molecules) to those containing both S2 and S3 (above 3.8 water molecules). If this is the case, then the relative site stoichiometries implied by the results of the present study are more consistent with Raman observations than are those of Fialips *et al.* (2005). In addition, except at very low water contents, our data are considerably more energetic than their results for S3 and the least energetic values for S2.

Figure 13 shows $\Delta\tilde{H}_{R,T,P}$ on a per mol chabazite basis as a function of water content calculated from $\Delta\bar{H}_{R,T,P}$ depicted in Figure 12. Shown for comparison are calculated values derived from the raw calorimetric results of Shim *et al.* (1999) and the thermodynamic model presented by Fialips *et al.* (2005) based on $\Delta\bar{H}_{R,T,P}$ shown in Figure 12. It can be seen that the integral heat results of this study are very similar in magnitude to those of Fialips *et al.* (2005). The topology is somewhat different, with the results of this study exhibiting a break in slope at ~4 water molecules per mol of chabazite, whereas those of Fialips *et al.* (2005) produce a smooth curve. This difference probably reflects the irreversible nature of the present results, as opposed to the equilibrium water molecule distribution assumed in the calculation from Fialips *et al.* (2005).

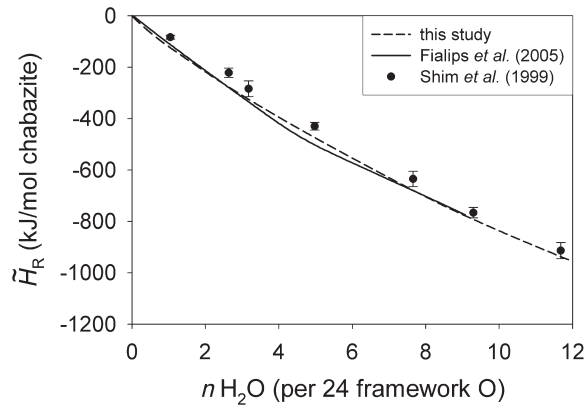

Figure 13. Integral molar enthalpy of hydration ($\Delta\tilde{H}_{R,T,P}$) of chabazite as a function of the number of water molecules per 24 framework oxygens based on the results of this study (solid curve), of Fialips *et al.* (2005; dashed curve), and of Shim *et al.* (1999; symbols).

The results of Shim *et al.* (1999) define a smooth curve almost parallel to that of this study and Fialips *et al.* (2005), though they are systematically less exothermic. Although the other results are more exothermic than those of Shim *et al.* (1999), it can be seen in Figure 13 that the topology of either the curve from this study or that of Fialips *et al.* (2005) would satisfy the constraints presented by the TTD data. This highlights the insensitivity of $\Delta\tilde{H}_{R,T,P}$ to energetic distinctions between sites, as the smooth fit suggested by Shim *et al.* (2005) to explain their data does not accurately depict the energetic distinctions present in water molecules at different degrees of infilling. This emphasizes the need to obtain direct $\Delta\bar{H}_{R,T,P}$ results, as is possible with the present technique or through regression of phase equilibrium observations.

CONCLUSIONS

The techniques of the present study afford a new and relatively easy approach for obtaining both partial and integral molar heat of hydration data for zeolites and other mineral hydrates as a function of composition and temperature. The accuracy of the results obtained through the present method is indicated by the favorable comparisons with existing data obtained through other calorimetric and phase equilibrium techniques. While each material presents its own set of challenges due to differences in the nature of water sites, the rate of hydration, and the range of hydration state obtainable under a given set of temperature and humidity conditions, judicious application of the data-handling techniques presented above affords a significant complement, and in many cases, an improvement to the quality of information about hydration energetics available with other techniques. This technique could also be adopted to measure heats of dehydration for materials whose hydration state varies appreciably within the range of vapor pressures attainable in the experimental setup. Specific strengths of this technique are: (1) unambiguous determination of the degree and range of hydration associated with calorimetric observations. This is typically a major source of error and uncertainty in other techniques (*e.g.* Muller *et al.*, 1998). (2) Direct, model-independent determination of partial molar heats of hydration as a function of hydration state. Most other calorimetric techniques (traditional liquid immersion calorimetry, heat of solution measurements) can only obtain this information through laborious measurement of integral heats over a range of composition. This technique can obtain this information at a given temperature in one experiment, without complications due to the choice of equation used to describe the compositional dependence of the integral heat data. (3) Heats of hydration in materials like analcime that absorb water very slowly can be determined with reasonable precision. (4) The variation in the heats of hydration with temperature can be determined directly through measurements at different temperatures. This application of the technique is explored in forthcoming papers on the materials described above. (5) Additional information can ideally be obtained from these experiments, including reaction rates as a function of degree of hydration and the equilibrium water content at the experimental temperature and water vapor pressure.

One main limitation of the present technique is that the range of humidity conditions obtainable in the DSC-TGA device is effectively limited by the equilibrium vapor pressure of H_2O at room temperature (~32 mbar; in practice lower vapor pressures are preferable so as to preclude condensation within the instrument). As saturated vapor pressure increases dramatically with increasing temperature (up to ~220 bar at the critical point), experiments at elevated temperature conducted with this technique are limited to vapor pressures far below saturation. This limits the extent of hydration possible for some materials at elevated temperatures, as observed in chabazite. Currently available simultaneous DSC-TGA instruments are all limited by this phenomenon, but future advances may extend this technique to higher vapor pressures. Until then, assessment of hydration states obtainable at higher humidity conditions must rely on extrapolation of results from lower temperature or regression of equilibrium observations at higher pressures, such as those obtained by Wilkin and Barnes (1999).

The limited humidity range accessible by the present technique also controls whether measurement of both hydration and dehydration heats at the same temperature is possible. In minerals like chabazite that exhibit a range of hydration states at elevated temperatures between 0 and 32 mbar (*e.g.* Fialips *et al.*, 2005), such measurements should be possible and would allow assessment of the reversibility. In minerals like natrolite that dehydrate over a very small range of temperature (*e.g.* van Reeuwijk, 1974), measurement of both hydration and dehydration heats is generally not feasible.

Another limitation is that partial molar heats of hydration at very low degrees of hydration are not possible, as shown by the very non-energetic values obtained at early stages in the hydration experiments (*cf.* Figures 5, 9, 12). The cause of this behavior is unclear, but probably, at least partly, reflects the energetics of exchange of N_2 gas (with which the samples were saturated) and H_2O at early stages of the experiments. This complication would be present in any gas absorption experiment on materials that absorb N_2, and in any equilibrium measurement made at very low water contents.

ACKNOWLEDGMENTS

This work was supported in part by the US National Science Foundation (grant EAR-0336906) to PSN. L. Ruhl and S. Keddy assisted with sample preparation. Reviews

by R. Wilkin and J.W. Carey led to significant improvements in the paper.

REFERENCES

Alberti, A. and Vezzalini, G. (1981) A partially disordered natrolite; relationships between cell parameters and Si-Al distribution. *Acta Crystallographica, Section B: Structural Crystallography and Crystal Chemistry*, **37**, 781–788.

Alberti, A. and Vezzalini, G. (1983) How the structure of natrolite is modified through the heating-induced dehydration. *Neues Jahrbuch für Mineralogie Monatshefte*, 135–144.

Alberti, A., Galli, E., Vezzalini, G., Passaglia, E. and Zanazzi, P.F. (1982) Position of cations and water-molecules in hydrated chabazite – natural and Na-exchanged, Ca-exchanged, Sr-exchanged and K-exchanged chabazites. *Zeolites*, **2**, 303–309.

Balgord, W.D. and Roy, R. (1973) Crystal chemical relationships in analcite Family. 2. Influence of temperature and pH_2O on structure. *Advances in Chemistry Series*, 189–199.

Barany, R. (1962) Heats and free energies of formation of some hydrated and anhydrous sodium- and calcium-aluminum silicates. *U.S. Bureau of Mines Report of Investigations*, no. 5900.

Barrer, R.M. and Cram, P.J. (1971) Heats of immersion of outgassed ion-exchanged zeolites. Pp. 105–131 in: *Molecular Sieve Zeolites-II* (R.F. Gould, editor). Advances in Chemistry Series 102, American Chemical Society, Washington, D.C.

Baur, W.H. and Joswig, W. (1996) The phases of natrolite during dehydration and rehydration studied by single crystal X-ray diffraction methods between room temperature and 923 K. *Neues Jahrbuch für Mineralogie Monatshefte*, **1996**, 171–187.

Bish, D.L. and Carey, J.W. (2001) Thermal behavior of natural zeolites. Pp. 403–452 in: *Natural Zeolites: Occurrences, Properties, Applications* (D.L. Bish and D.W. Ming, editors). Reviews in Mineralogy and Geochemistry, **45**, Mineralogical Society of America and the Geochemical Society, Washington, D.C.

Bish, D.L., Carey, J.W., Vaniman, D.T. and Chipera, S.J. (2003a) Stability of hydrous minerals on the Martian surface. *Icarus*, **164**, 96–103.

Bish, D.L., Vaniman, D.T., Chipera, S.J. and Carey, J.W. (2003b) The distribution of zeolites and their effects on the performance of a nuclear waste repository at Yucca Mountain, Nevada, USA. *American Mineralogist*, **88**, 1889–1902.

Boddenberg, B., Rakhmatkariev, G.U., Hufnagel, S. and Salimov, Z. (2002) A calorimetric and statistical mechanics study of water adsorption in zeolite NaY. *Physical Chemistry Chemical Physics*, **4**, 4172–4180.

Cammenga, H.K., Eysel, W., Gmelin, E., Hemminger, W., Hohne, G.W.H. and Sarge, S.M. (1993) The temperature calibration of scanning calorimeters. 2. Calibration substances. *Thermochimica Acta*, **219**, 333–342.

Carey, J.W. (1993) The heat-capacity of hydrous cordierite above 295 K. *Physics and Chemistry of Minerals*, **19**, 578–583.

Carey, J.W. and Bish, D.L. (1996) Equilibrium in the clinoptilolite-H_2O system. *American Mineralogist*, **81**, 952–962.

Carey, J.W. and Bish, D.L. (1997) Calorimetric measurement of the enthalpy of hydration of clinoptilolite. *Clays and Clay Minerals*, **45**, 826–833.

Chipera, S.J. and Bish, D.L. (1991) Rehydration behavior of natural analcime. *Clay Minerals Society, 28th Annual Meeting, Program and Abstracts, Houston, Texas,* p. 29.

Cruciani, G. and Gualtieri, A. (1999) Dehydration dynamics of analcime by in situ synchrotron powder diffraction. *American Mineralogist*, **84**, 112–119.

Drebushchak, V.A. (1999) Measurements of heat of zeolite dehydration by scanning heating. *Journal of Thermal Analysis and Calorimetry*, **58**, 653–662.

Fialips, C.I., Carey, J.W. and Bish, D.L. (2005) Hydration-dehydration behavior and thermodynamics of chabazite. *Geochimica et Cosmochimica Acta*, **69**, 2293–2308.

Fridriksson, T., Carey, J.W., Bish, D.L., Neuhoff, P.S. and Bird, D.K. (2003) Hydrogen-bonded water in laumontite II: Experimental determination of site-specific thermodynamic properties of hydration of the W1 and W5 sites. *American Mineralogist*, **88**, 1060–1072.

Gatta, G.D. (1985) Direct determination of adsorption heats. *Thermochimica Acta*, **96**, 349–363.

Gmelin, E. and Sarge, S.M. (2000) Temperature, heat and heat flow rate calibration of differential scanning calorimeters. *Thermochimica Acta*, **347**, 9–13.

Gualtieri, A.F. (2000) Accuracy of XRPD QPA using the combined Rietveld-RIR method. *Journal of Applied Crystallography*, **33**, 267–278.

Guliev, T.M., Isirikyan, A.A., Mirzai, D.I. and Serpinskii, V.V. (1989) Energy of rehydration of natrolite and scolecite. *Bulletin of the Academy of Sciences of the USSR Division of Chemical Science*, **37**, 1308–1310.

Hey, M.H. (1932) Studies on the zeolites. Part III. Natrolite and metanatrolite. *Mineralogical Magazine*, **23**, 243–289.

Höhne, G.W.H., Cammenga, H.K., Eysel, W., Gmelin, E. and Hemminger, W. (1990) The temperature calibration of scanning calorimeters. *Thermochimica Acta*, **160**, 1–12.

Johnson, G.K., Flotow, H.E., Ohare, P.A.G. and Wise, W.S. (1982) Thermodynamic studies of zeolites – analcime and dehydrated analcime. *American Mineralogist*, **67**, 736–748.

Johnson, G.K., Tasker, I.R., Jurgens, R. and Ohare, P.A.G. (1991) Thermodynamic studies of zeolites – clinoptilolite. *Journal of Chemical Thermodynamics*, **23**, 475–484.

Johnson, G.K., Tasker, I.R., Flotow, H.E., Ohare, P.A.G. and Wise, W.S. (1992) Thermodynamic studies of mordenite, dehydrated mordenite, and gibbsite. *American Mineralogist*, **77**, 85–93.

Kasai, T., Maeda, H., Matsui, K., Kurnia, D.F., Nakayama, N. and Mizota, T. (1994) Hydration enthalpy for synthetic and cation exchanged A-type zeolites with special reference to zeolite heat pump media. *Mineralogical Journal*, **17**, 170–180.

Kiseleva, I., Navrotsky, A., Belitsky, I.A. and Fursenko, B.A. (1996a) Thermochemistry and phase equilibria in calcium zeolites. *American Mineralogist*, **81**, 658–667.

Kiseleva, I., Navrotsky, A., Belitsky, I.A. and Fursenko, B.A. (1996b) Thermochemistry of natural potassium sodium calcium leonhardite and its cation-exchanged forms. *American Mineralogist*, **81**, 668–675.

Kiseleva, I., Ogorodova, L.P., Melchakova, L.V., Belitsky, I.A. and Fursenko, B.A. (1997) Thermochemical investigation of natural fibrous zeolites. *European Journal of Mineralogy*, **9**, 327–332.

Kiseleva, I., Navrotsky, A., Belitsky, I.A. and Fursenko, B.A. (2001) Thermochemical study of calcium zeolites; heulandite and stilbite. *American Mineralogist*, **86**, 448–455.

Long, J.C.S. and Ewing, R.C. (2004) Yucca Mountain: Earth-science issues at a geologic repository for high-level nuclear waste. *Annual Review of Earth and Planetary Sciences*, **32**, 363–401.

Mazzi, F. and Galli, E. (1978) Is each analcime different? *American Mineralogist*, **63**, 448–460.

Meier, W.M. (1960) The crystal structure of natrolite. *Zeitschrift für Kristallographie*, **113**, 430–444.

Mizota, T., Matsui, K., Kasai, T. and Nakayama, N. (1995)

Hydration enthalpies of synthetic Na-A, cation-exchanged-A and some natural zeolites for evaluating as heat exchange absorbents. *Thermochimica Acta*, **266**, 331–341.

Muller, J.C.M., Hakvoort, G. and Jansen, J.C. (1998) DSC and TG study of water adsorption and desorption on zeolite NaA – Powder and attached as layer on metal. *Journal of Thermal Analysis and Calorimetry*, **53**, 449–466.

Neuhoff, P.S. and Bird, D.K. (2001) Partial dehydration of laumontite: Thermodynamic constraints and petrogenetic implications. *Mineralogical Magazine*, **65**, 59–70.

Neuhoff, P.S. and Wang, J. (2007) Heat capacity of hydration in zeolites. *American Mineralogist*, in press.

Neuhoff, P.S., Fridriksson, T. and Bird, D.K. (2000) Zeolite parageneses in the North Atlantic igneous province; implications for geotectonics and groundwater quality of basaltic crust. *International Book Series*, **5**, 271–300.

Neuhoff, P.S., Kroeker, S., Du, L.-S., Fridriksson, T. and Stebbins, J.F. (2002) Order/disorder in natrolite group zeolites: A ^{29}Si and ^{27}Al MAS NMR study. *American Mineralogist*, **87**, 1307–1320.

Neuhoff, P.S., Stebbins, J.F. and Bird, D.K. (2003) Si-Al disorder and solid solutions in analcime, chabazite and wairakite. *American Mineralogist*, **88**, 410–423.

Ogorodova, L.P., Kiseleva, I.A., Melchakova, L.V., Belitskii, I.A. and Fursenko, B.A. (1996) Enthalpies of formation and dehydration of natural analcime. *Geochemistry International*, **34**, 980–984.

Ogorodova, L.P., Kiseleva, I.A., Mel'chakova, L.V. and Belitskii, I.A. (2002) Thermodynamic properties of calcium and potassium chabazites. *Geochemistry International*, **40**, 466–471.

Otsuka, R., Yamazaki, A. and Kato, K. (1991) Kinetics and mechanism of dehydration of natrolite and its potassium exchanged form. *Thermochimica Acta*, **181**, 45–56.

Pechar, F., Schaefer, W. and Will, G. (1983) A neutron diffraction refinement of the crystal structure of natural natrolite, $Na_2Al_2Si_3O_{10}\cdot 2H_2O$. *Zeitschrift für Kristallographie*, **164**, 19–24.

Petrova, N., Mizota, T. and Fujiwara, K. (2001) Hydration heats of zeolites for evaluation of heat exchangers. *Journal of Thermal Analysis and Calorimetry*, **64**, 157–166.

Pires, J., de Carvalho, M.B., Carvalho, A.P., Guil, J.M. and Perdigon-Melon, J.A. (2000) Heats of adsorption of N-hexane by thermal gravimetry with differential scanning calorimetry (TG-DSC): A tool for textural characterization of pillared clays. *Clays and Clay Minerals*, **48**, 385–391.

Robie, R.A. and Hemingway, B.S. (1995) Thermodynamic properties of minerals and related substances at 298.15 K and 1 bar (105 pascals) pressure and at higher temperatures. *United States Geological Survey Bulletin*, **2131**, 461 pp.

Sabbah, R., An, X.W., Chickos, J.S., Leitao, M.L.P., Roux, M.V. and Torres, L.A. (1999) Reference materials for calorimetry and differential thermal analysis. *Thermochimica Acta*, **331**, 93–204.

Sarge, S.M., Gmelin, E., Hohne, G.W.H., Cammenga, H.K., Hemminger, W. and Eysel, W. (1994) The caloric calibration of scanning calorimeters. *Thermochimica Acta*, **247**, 129–168.

Shim, S.H., Navrotsky, A., Gaffney, T.R. and MacDougall, J.E. (1999) Chabazite: Energetics of hydration, enthalpy of formation, and effect of cations on stability. *American Mineralogist*, **84**, 1870–1882.

Smyth, J.R. (1982) Zeolite stability constraints on radioactive-waste isolation in zeolite-bearing volcanic-rocks. *Journal of Geology*, **90**, 195–201.

Stolen, S., Glockner, R. and Gronvold, F. (1996) Heat capacity of the reference material synthetic sapphire (α-Al_2O_3) at temperatures from 298.15 K to 1000 K by adiabatic calorimetry. Increased accuracy and precision through improved instrumentation and computer control. *Journal of Chemical Thermodynamics*, **28**, 1263–1281.

Tchernev, D.I. (2001) Natural zeolites in solar energy heating, cooling, and energy storage. Pp. 589–617 in: *Natural Zeolites: Occurrences, Properties, Applications* (D.L. Bish and D.W. Ming, editors). Reviews in Mineralogy and Geochemistry, **45**, Mineralogical Society of America and the Geochemical Society, Washington, D.C.

Tingle, T.N., Neuhoff, P.S., Ostergren, J.D., Jones, R.E. and Donovan, J.J. (1996) The effect of "missing" (unanalyzed) oxygen on quantitative electron probe microanalysis of hydrous silicate and oxide minerals. *Geological Society of America, 28th annual meeting, Boulder, Colorado*, p. 212.

Valueva, G.P. and Goryainov, S.V. (1992) Chabazite during dehydration (thermochemical and Raman spectroscopy study). *Russian Geology and Geophysics*, **33**, 68–75.

van Reeuwijk, L.P. (1972) High-temperature phases of zeolites of the natrolite group. *American Mineralogist*, **57**, 499–510.

van Reeuwijk, L.P. (1974) *The Thermal Dehydration of Natural Zeolites*. H. Veenman and Zonen B.V., Wageningen, The Netherlands, 88 pp.

Wilkin, R.T. and Barnes, H.L. (1998) Solubility and stability of zeolites in aqueous solution: I. Analcime, Na- and K-clinoptilolite. *American Mineralogist*, **83**, 746–761.

Wilkin, R.T. and Barnes, H.L. (1999) Thermodynamics of hydration of Na- and K-clinoptilolite to 300ºC. *Physics and Chemistry of Minerals*, **26**, 468–476.

Yang, S.Y. and Navrotsky, A. (2000) Energetics of formation and hydration of ion-exchanged zeolite Y. *Microporous and Mesoporous Materials*, **37**, 175–186.

Yang, S.Y., Navrotsky, A. and Wilkin, R.T. (2001) Thermodynamics of ion-exchanged and natural clinoptilolite. *American Mineralogist*, **86**, 438–447.

(*Received 8 September 2006; revised 2 January 2007; Ms. 1216, Guest Associate Editor Thomas Armbruster*)